Modelling the thermoelectric properties of cement-based materials using finite element method and effective medium theory

13 authors, including:

Conrad S.N. Johnston
Pacific Northwest National Laboratory
14 PUBLICATIONS   185 CITATIONS

SEE PROFILE

Piotr Chudzinski
Queen's University Belfast
52 PUBLICATIONS   632 CITATIONS

SEE PROFILE

Esther Orisakwe
Queen's University Belfast
11 PUBLICATIONS   65 CITATIONS

SEE PROFILE

Some of the authors of this publication are also working on these related projects:

Project   Daylighting and Thermo-Electrical performance of an Autonomous Suspended Particle Device Evacuated Glazing View project

Project   Evaluation of PDLC glazing for low energy building View project

Modelling the thermoelectric properties of cement-based materials using finite element method and effective medium theory

Lorenzo Stella[1,2], Conrad Johnston[3], Javier F. Troncoso[4], Piotr Chudzinski[1,5], Esther Orisakwe[1], Jorge Kohanoff[6,1], Ruchita Jani[7], Niall Holmes[7], Brian Norton[8], Xiaoli Liu[9], Ming Qu[9], Hongxi Yin[10], Kazuaki Yazawa[11]

[1]School of Mathematics and Physics, Queen's University Belfast, UK
[2]School of Chemistry and Chemical Engineering, Queen's University Belfast, UK
[3]Pacific Northwest National Laboratory, Richland, WA, USA
[4]Swiss Federal Laboratories for Materials Science and Technology (EMPA), Thun, Switzerland
[5]Institute of Fundamental Technological Research, Polish Academy of Sciences, Warsaw, Poland
[6]Instituto de Fusion Nuclear "Guillermo Velarde", Universidad Politecnica de Madrid, Spain
[7]School of Civil and Structural Engineering, Technological University Dublin, Ireland
[8]Tyndall National Institute, Cork, Ireland
[9]Lyles School of Civil Engineering, Purdue University, West Lafayette, IN, USA
[10]International Center for Energy, Environment & Sustainability, Washington University in St Louis (WUST), St Louis, MO, USA
[11]Birck Nanotechnology Center, Purdue Univeristy, West Lafayette, IN, USA

email: l.stella@qub.ac.uk, conrad.johnston@pnnl.gov, javier.fernandez@empa.ch, niall.holmes@tudublin.ie, p.chudzinski@qub.ac.uk, e.orisakwe@qub.ac.uk, j.kohanoff@upm.es, d18126665@mytudublin.ie, brian.norton@tyndall.ie, liu2251@purdue.edu, mqu@purdue.edu, hongxi.yin@wustl.edu, kyazawa@purdue.edu

ABSTRACT: Because of the thermoelectric (TE) effect (or Seebeck effect), a difference of potential is generated as a consequence of a temperature gradient across a sample. The TE effect has been mostly studied and engineered in semiconducting materials and it already finds several commercial applications. Only recently the TE effect in cement-based materials has been demonstrated and there is a growing interest in its potential. For instance, a temperature gradient across the external walls of a building can be used to generate electricity. By the inverse of the TE effect (or Peltier effect), one can also seek to control the indoor temperature of a building by biasing TE elements embedded in its external walls. In designing possible applications, the TE properties of cement-based materials must be determined as a function of their chemical composition. For instance, the TE properties of cement paste can be enhanced by the addition of metal oxide (*e.g.*, Fe_2O_3) powder. In this paper, a single thermoelectric leg is studied using the finite element method. Metal oxide additives in the cement paste are modelled as spherical inhomogeneities. The thermoelectric properties of the single components are based on experimental data, while the overall thermoelectric properties of the composites are obtained from the numerical model. The results of this numerical study are interpreted according to the effective medium theory (EMT) and its generalisation (GEMT).

KEY WORDS: Cement composites; Thermoelectrics; Seebeck Coefficient; Electrical Conductivity; Thermal Conductivity.

1 INTRODUCTION

Cement-based thermoelectric composites are a novel class of "smart" materials with several potential applications.[1-4] For instance, by means of the Seebeck effect, a temperature gradient across the external walls of a building can be used to generate electricity.

For open circuit conditions, the difference of electric potential, ΔV, established between the two ends of a conductor kept at different temperatures depends on the temperature difference, ΔT, and on a characteristic material property, the Seebeck coefficient, $S = -\Delta V/\Delta T$. In this paper, all Seebeck coefficients are absolute,[5] *i.e.*, they tend to zero as the temperature approaches 0 K, unless stated differently. The Seebeck coefficient of plain (*i.e.*, without additives) hydrated cement paste has been reported as either small (ranging from $S_{\text{cement}} = -1$ μV/K[6] to $S_{\text{cement}} = +2.69$ μV/K[7, 8]) or negligible ($S_{\text{cement}} = 10^{-4} - 10^{-5}$ μV/K[9]). The introduction of a small fraction of additives (usually a few wt%, mixed in dry condition) into the cement paste can largely enhance the magnitude of its Seebeck coefficient.

Wei *et al*. showed an effective Seebeck coefficient, $S_{eff} = +22.07$ μV/K, in Carbon Fibre Reinforced Cement (CFRC) composites with 1.0 wt% carbon fibre.[10] Addition of Expanded Graphite (EG) to CFRC composite gives a maximum $S_{eff} = +11.59$ μV/K at 33 °C.[11] In this case it has been observed a dependence of the effective Seebeck coefficient on moisture content. The authors also showed that in purely Expanded Graphite Cement Composites (EGCC), a $S_{eff} = +20.0$ μV/K can be achieved.[9]

Addition of oxide nanoparticles to CFRC composites boosted the values of the effective Seebeck coefficient of the composite to $S_{eff} = +92.57$ μV/K with 5 wt% Fe_2O_3 or to $S_{eff} = +100.28$ μV/K with 5 wt% Bi_2O_3.[12] Despite the leap in the Seebeck coefficient, the overall figure of merit is only slightly increased because of the limited increase in electrical conductivity upon addition of semiconducting oxides.[12, 13] Ji *et al.* have obtained a stunning $S_{eff} = +2,500$ μV/K for cement-based composites with 5 wt% Fe_2O_3 nanoparticles and $S_{eff} = +3,300$ with 5 wt% Bi_2O_3 nanoparticles, while Ji et *al*. have obtained $S_{eff} = -3,085$ μV/K with 5 wt% MnO_2 nanoparticles.[14] This result has been recently extended to

carbon fibre/MnO$_2$ composite for which a value of $S_{eff} = -2,800$ µV/K with 8 wt% fibre/MnO$_2$ content has been achieved.[15] In this composite, a largely increased overall figure of merit has been also reported, owing to the good electrical conductivity due to the carbon fibre content.

Despite the growing experimental evidence, numerical models of the thermoelectric properties of cement-based composite materials are scarce.[16]

Assuming that the thermoelectric properties of each component are known, the effective medium theory (EMT),[17] or its generalisation (GEMT),[18-21] can be used to assess the properties of the composite material. Both EMT and GEMT model a composite as a "pseudo-homogenous" material and do not require the microscopic knowledge of the oxide additive distribution. Since the microscopic scale of the composite must not be resolved, models based on either EMT or GEMT are expected to scale more favourably towards real-size (*i.e.*, a few centimetres across[22]) thermoelectric units. To this end, numerical know-how from FEM modelling of traditional thermoelectric units is available, [22-29] and can be easily customised by changing the material properties, when known.

Before applying either EMT or GEMT with confidence to cement-based material, some preliminary validation is in order. In this paper, we have modelled the thermoelectric properties of a cement-based composite material with microscopic resolution and compared the results against the EMT and GEMT predictions.

Ferric oxide, Fe$_2$O$_3$, has been used as a representative of the class of oxide materials present in the experimental literature. Simple EMT does not provide a good fit of the properties determined by the microscopic modelling. Although GEMT seems to be more accurate, discrepancies in the fitting of cement-based composite in the saturated and dry conditions suggest some caution. Discrepancies may be due to the averaging procedure used to determine the effective Seebeck coefficient of the cement-based composite material.

2   MATERIAL MODELLING

We model cement-based composites with ferric oxide, Fe$_2$O$_3$, as a typical oxide additive. Also known with the name of the naturally occurring mineral hematite, Fe$_2$O$_3$ is a semiconductor oxide. At room temperature, the electronic conductivity (unit: S/m) of Fe$_2$O$_3$ is extrinsic and the majority carriers are electrons.[30] The electron mobility, $\mu_{Fe_2O_3}$ (unit: cm^2/V·s), is activated and it depends on temperature, T (unit: K), as

$$\mu_{Fe_2O_3}(T) = (1.998 \cdot 10^5/T)\exp(-0.17/k_B T),$$

where $k_B = 8.617 \cdot 10^{-5}$ eV/K is the Boltzmann constant. The activation energy, 0.17 eV, is appropriate at low temperature ($T < 923$ K).[30] The electrical conductivity is then written as

$$\sigma_{Fe_2O_3}(T) = eN_D\mu_{e,Fe_2O_3}(T),$$

where $e = 1.602 \cdot 10^{-19}$ C is the unit of charge and $N_D = 10^{19}$ cm^{-3} is the notional value of the donor concentration used in this work. For this value of the concentration, $\sigma_{Fe_2O_3}(298.15$ K$) = 1.436$ S/m. No precise assessment of the donor concentration has been found in the literature for the Fe$_2$O$_3$ microparticles used in cement-based composites.

The Seebeck coefficient also shows a temperature dependence typical of a semiconductor,

$$S_{Fe_2O_3}(T) = -\left(\frac{k_B}{e}\right)\left[\left(\frac{0.17}{k_B T}\right) + g\right],$$

where $g = 3$ for carrier relaxation processes determined by optical phonons scattering.[31] In particular, $S_{Fe_2O_3}(298.15$ K$) = -828.7$ µV/K.

We also used the value $\rho_{Fe_2O_3} = 5.26$ g/cm^3 for the density and $\kappa_{Fe_2O_3} = 12.55$ W/m·K for the thermal conductivity of Fe$_2$O$_3$. The temperature dependence of these quantities has been neglected.

For the dry cement powder, we have used a density of 3.1 g/cm^3. The density of the hydrated (0.4 water/cement ratio) cement paste with a notional 0.2 porosity is $\rho_{cement} = 2.0$ g/cm^3. The values of the electrical conductivity, thermal conductivity and Seebeck coefficient of the plain (*i.e.*, with no oxide additives) hydrated cement paste have been taken from Jani *et al.*[6] They are $\sigma_{cement,sat.} = 0.07$ S/m, $\kappa_{cement} = 1.15$ W/m·K and $S_{cement} = -1$ µV/K, where the value of the electrical conductivity corresponds to the pore saturation condition. A much lower value of electrical conductivity, $\sigma_{cement,dry} = 2 \cdot 10^{-4}$ S/m, has been reported for dry hydrated cement paste. All quantities are given at room temperature.

The cement-based composite is modelled as a collection of spherical Fe$_2$O$_3$ microparticles inside a matrix of plain hydrated cement paste. The diameter of the spheres is set to 50 µm and superposition between spheres is allowed. Allowing for superposition partially compensates for the lack of dispersion in sphere diameters. In practice, the coordinates of the centre of each sphere are chosen at random within the volume of the composite. A "switch" function, $\phi(x,y,z)$, is defined to smoothly (as a cubic polynomial) interpolate between the value "1" inside each sphere and the value "0" in the matrix. The switch function is then used to define the local properties of the composite, *e.g.*, the local Seebeck coefficient of the composite is defined as

$$S_{comp}(x,y,z) = S_{cement} + \left(S_{Fe_2O_3} - S_{cement}\right)\phi(x,y,z)$$

and the local electrical conductivity as

$$\sigma_{comp}(x,y,z) = \sigma_{cement} + \left(\sigma_{Fe_2O_3} - \sigma_{cement}\right)\phi(x,y,z).$$

The model includes copper contacts at the two ends of the cement-based composite (see Fig.1). The Cu contacts facilitate the implementation of the boundary conditions, especially the open circuit condition. The relevant material properties are $\rho_{Cu} = 8.69$ g/cm^3 for the density, $\kappa_{Cu} = 400$ W/m·K for the thermal conductivity, $\sigma_{Cu} = 5.998 \cdot 10^7$ S/m for the electric conductivity, and $S_{Cu} = 1.83$ V/K for the Seebeck coefficient.[5]

3   COMPUTATIONAL METHODS

The coupled charge and heat transport equations for the geometry shown in Fig. 1 have been solved by means of the Finite Element Method (FEM) as implemented in COMSOL Multiphysics® (version 6.0).[32]
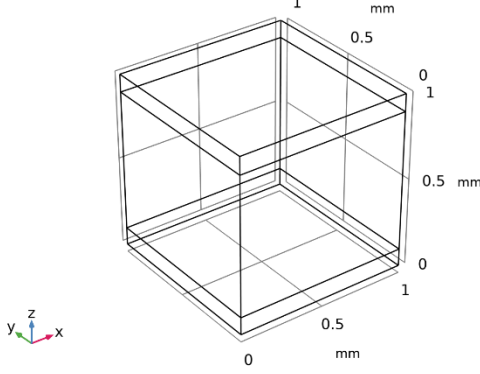

Figure 1. Model geometry. The first surface is the bottom one. The second surface is the interface between the lower Cu electrode and the cement-base composite. The third surface is the interface between the cement-base composite and the upper Cu electrode. The fourth surface is the top one.

The transport equations are:
$$\begin{cases} \nabla \cdot \boldsymbol{J} = 0, \\ \nabla \cdot (-\kappa \nabla T + ST\boldsymbol{J}) = -\boldsymbol{J} \cdot \nabla V, \end{cases}$$
where the electrical potential, V, and the temperature, T, are the unknown fields, and $\boldsymbol{J} = -\sigma \nabla V - \sigma S \nabla T$ is the thermoelectric current density. Because of the thermoelectric effect, the current depends on the gradients of both the electrical potential and the temperature.
The boundary conditions for the model are: $T_{in} = 298.15$ K and $V_{in} = 0$ (ground) on the lower Cu electrode surface, $T_{out} = 298.15 + \Delta T$ (K) and $\boldsymbol{J} \cdot \boldsymbol{n} = 0$ (open circuit) on the upper Cu electrode surface, where $\boldsymbol{n}$ is the normal vector to that surface. We consider three values $\Delta T = 0.1, 0.5, 1.0$ K and then extrapolate to the limit of $\Delta T \to 0$ to compute the effective Seebeck coefficient. Natural boundary conditions for both the electrical potential and temperature are imposed on the lateral surfaces.
Geometries containing different numbers, N_s, of spherical oxide microparticles have been generated. We considered the following values: $N_s = 0$, 100, 200, 300, 400, 500, 600, 700, 800, 900, 1000, 2000, 3000, 4000, 5000, 6000, 7000, 8000, 9000, 10000, and 100000. The cases $N_s = 0$ and $N_s = 100,000$ spherical microparticles give the extreme cases of plain hydrated cement paste and pure Fe_2O_3, respectively. A switch function $\phi(x, y, z)$ is generated for each of the cases above and stored on a discretised $100 \times 100 \times 100$ cubic grid. The volume fraction is defined as the average of the "switch" function over the cement-based composite volume. A cubic $50 \times 50 \times 50$ mesh for the whole geometry has been used for all the FEM calculations.

4   RESULTS

The effective Seebeck coefficient of the cement-based composite is estimated as

$$S_{eff} = -\frac{\bar{V}_3 - \bar{V}_2}{\bar{T}_3 - \bar{T}_2},$$

where $\bar{V}_{2,3}$ and $\bar{T}_{2,3}$ are the averages of the electric potential and temperature taken over the second and third surfaces, respectively (see Fig. 1). An estimate of S_{eff} is obtained for each value of ΔT. Note that the isosurfaces of the temperature (see Fig. 2) and of the electric potential (see Fig. 3) are not necessarily parallel and depend on the oxide microparticles distribution. This lack of homogeneity introduces a finite variance in the averages $\bar{V}_{2,3}$ and $\bar{T}_{2,3}$, and a consequent error in the estimator.
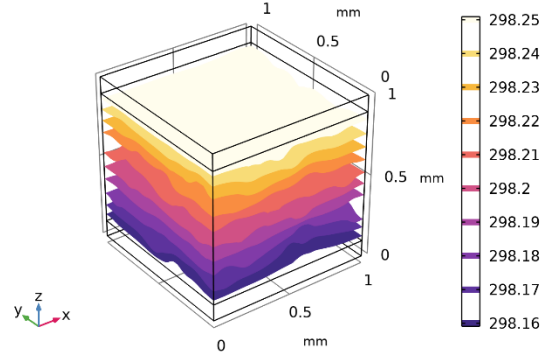

Figure 2. Temperature isosurfaces corresponding to volume fraction of Fe_2O_3 equal to 0.22. The temperature difference between the upper and lower surfaces is $\Delta T = 0.1$ K.
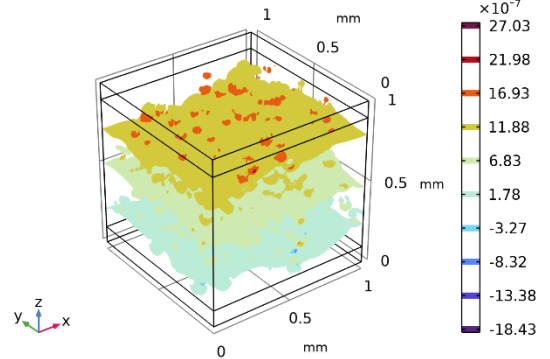

Figure 3. Electric potential isosurfaces corresponding to volume fraction of Fe_2O_3 equal to 0.22. The temperature difference between the upper and lower surfaces is $\Delta T = 0.1$ K.

Numerical results from the FEM calculations are reported in Table 1 and shown in Fig. 4 and 5. Those values have been obtained by extrapolating the numerical values S_{eff} for $\Delta T \to 0$. As expected, the value of the effective Seebeck coefficient grows monotonically with the oxide volume fraction. The values of S_{eff} for dry conditions are always larger than those for saturated conditions. In our model these conditions are only distinguished by the electrical conductivity of the cement paste. For dry conditions the electrical conductivity of the cement paste is much lower than that of the oxide additive. To explain the larger value of S_{eff} for dry conditions, one can tentatively assume that the effective Seebeck coefficient is a "weighted average" of the Seebeck coefficients of the single components.

If the "weight" is proportional to the electrical conductivity of the single components, the Seebeck coefficient of the oxide --- which is larger than that of the hydrated cement paste --- will be given a larger "weight" in the "weighted average" because its electrical conductivity is larger than that of the hydrated cement paste.

We have verified this explanation by computing the "weighted" average Seebeck coefficient, defined as

$$S_{ave} = \frac{\int S_{comp}(x,y,z)\sigma_{comp}(x,y,z)\mathrm{d}V}{\int \sigma_{comp}(x,y,z)\,\mathrm{d}V},$$

where the integrals extend over the volume occupied by the cement-based composite. The values of S_{ave} are reported in Fig. 4 and 5 (blue stars). Although they follow the same trend as S_{eff}, at least qualitatively, there are significant discrepancies.

Table 1. Effective Seebeck coefficients of the cement-based composite with different fractions of Fe_2O_3 microparticles. Values for both saturated and dry conditions are shown for comparison.

Number of microparticles	Volume fraction	Mass fraction	S_{eff} (Sat.) [μV/K]	S_{eff} (Dry) [μV/K]
0	0.00	0.00	-1.00	-1.01
100	0.05	0.14	-3.72	-13.0
200	0.09	0.23	-6.03	-24.3
300	0.15	0.34	-10.3	-43.9
400	0.18	0.40	-12.5	-54.2
500	0.22	0.45	-15.7	-71.0
600	0.26	0.50	-20.0	-91.2
700	0.29	0.55	-24.5	-111
800	0.34	0.61	-30.7	-138
900	0.36	0.63	-32.4	-146
1,000	0.39	0.66	-38.0	-171
2,000	0.63	0.83	-91.0	-372
3,000	0.77	0.91	-158	-539
4,000	0.86	0.95	-228	-651
5,000	0.92	0.97	-340	-729
6,000	0.94	0.98	-440	-759
7,000	0.97	0.99	-561	-787
8,000	0.98	0.99	-667	-803
9,000	0.99	1.00	-722	-812
10,000	0.99	1.00	-783	-821
100,000	1.00	1.00	-829	-829

The estimates for the effective Seebeck coefficient, S_{eff}, from the EMT are obtained by solving the equation[19-21]

$$f_{Fe_2O_3}\frac{\left(\frac{\sigma_{Fe_2O_3}}{S_{Fe_2O_3}}\right) - \left(\frac{\sigma_{eff}}{S_{eff}}\right)}{\left(\frac{\sigma_{Fe_2O_3}}{S_{Fe_2O_3}}\right) + 2\left(\frac{\sigma_{eff}}{S_{eff}}\right)} + f_{cement}\frac{\left(\frac{\sigma_{cement}}{S_{cement}}\right) - \left(\frac{\sigma_{eff}}{S_{eff}}\right)}{\left(\frac{\sigma_{cement}}{S_{cement}}\right) + 2\left(\frac{\sigma_{eff}}{S_{eff}}\right)} = 0,$$

where the effective electrical conductivity, σ_{eff}, is obtained by solving the equation

$$f_{Fe_2O_3}\frac{\sigma_{Fe_2O_3} - \sigma_{eff}}{\sigma_{Fe_2O_3} + 2\sigma_{eff}} + f_{cement}\frac{\sigma_{cement} - \sigma_{eff}}{\sigma_{cement} + 2\sigma_{eff}} = 0,$$

where $f_{Fe_2O_3}$ and f_{cement} are the volume fractions of the oxide and hydrated cement paste, respectively. There are no free parameters in the EMT and the theory should be applicable to the case of spherical inclusions.[17, 18] From the EMT, one expects a sharp percolation threshold at $f_c = 1/3$, if the electrical conductivity of the additive component is much larger than that of the host component.[18] This is supposed to be the case for dry conditions, but the sharp percolation threshold predicted by the EMT is not observed in our numerical results. This is a rather puzzling finding which casts some doubt on the accuracy of the numerical estimates of the effective Seebeck coefficient used in this work.

To gain some further insight, we tried to fit the numerical results using the GEMT. The theory has two free parameters, A and t.[18] In particular, the percolation threshold is related to the parameter A by the equation: $f_c = 1/(A+1)$. The estimates for the effective Seebeck coefficient, S_{eff}, from the GEMT are obtained by solving the equations[19-21]

$$f_{Fe_2O_3}\frac{\left(\frac{\sigma_{Fe_2O_3}}{S_{Fe_2O_3}}\right)^t - \left(\frac{\sigma_{eff}}{S_{eff}}\right)^t}{\left(\frac{\sigma_{Fe_2O_3}}{S_{Fe_2O_3}}\right)^t + A\left(\frac{\sigma_{eff}}{S_{eff}}\right)^t} + f_{cement}\frac{\left(\frac{\sigma_{cement}}{S_{cement}}\right)^t - \left(\frac{\sigma_{eff}}{S_{eff}}\right)^t}{\left(\frac{\sigma_{cement}}{S_{cement}}\right)^t + A\left(\frac{\sigma_{eff}}{S_{eff}}\right)^t} = 0,$$

where the effective electrical conductivity, σ_{eff}, is obtained by solving the equation

$$f_{Fe_2O_3}\frac{\left(\sigma_{Fe_2O_3}\right)^t - \left(\sigma_{eff}\right)^t}{\left(\sigma_{Fe_2O_3}\right)^t + A\left(\sigma_{eff}\right)^t} + f_{cement}\frac{\left(\sigma_{cement}\right)^t - \left(\sigma_{eff}\right)^t}{\left(\sigma_{cement}\right)^t + A\left(\sigma_{eff}\right)^t} = 0.$$

The EMT is retrieved from the GEMT when $A = 2$ and $t = 1$. A satisfactory, yet not perfect, fit of the numerical results for dry conditions is obtained by setting $A = 10^4$ and $t = 3.3$ in the GEMT (see Fig. 5). Such a large value of A corresponds to a percolation threshold $f_c \approx 0$, i.e., no percolation at all. Once again this is a puzzling result and may indicate a systematic bias in the estimator used to compute S_{eff}. The same values of the parameters A and t do not yield an equivalently satisfactory fit of the numerical results for the saturated condition (see Fig. 4). Finally, a large value of the GEMT parameter t is also unexpected, as $t = 1$ is usually appropriate for spherical inclusions.[18] As a comparison, two dimensional model based on Random Resistor Networks are in perfect agreement with the GEMT predictions.[33, 34]
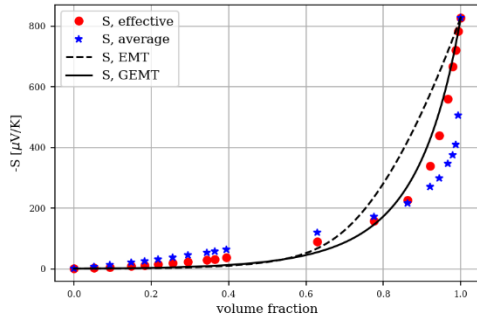
Figure 4. Negative effective Seebeck coefficient (red dots) and negative average Seebeck coefficient (blue dots) as a function of the volume fraction for saturated conditions. The EMT and best GEMT estimates ($A = 10^4$ and $t = 3.3$) are also reported.
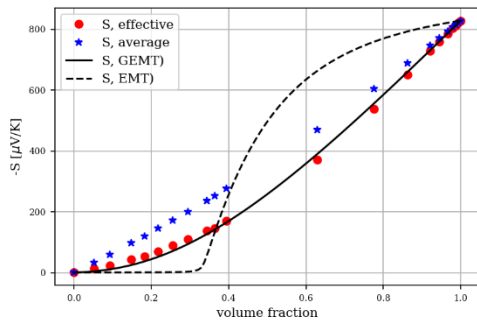

Figure 5. Same as Figure 4, but for dry conditions.

5   DISCUSSION AND CONCLUSIONS

In this paper we have shown preliminary numerical results for the calculation of the effective Seebeck coefficient, S_{eff}, of a cement-based composite material. To this end, a microscopic model of spherical Fe_2O_3 microparticles included into a matrix of hydrated cement paste has been solved by means of the Finite Element Method (FEM) as implemented in COMSOL Multiphysics® (version 6.0). Our numerical results follow the expected qualitative trend with an increasing volume fraction of oxide additives, but they do not display the percolation threshold expected for dry conditions.

A good agreement with the Effective Medium Theory (EMT) was also expected for spherical inclusions, but our results strongly deviate from the EMT predictions for both dry and saturated conditions. Relatively satisfactory regression of the numerical results by means of the Generalised Effective Medium Theory (GEMT) have been obtained, although for rather unphysical values of the GEMT parameters.

While further numerical validation is in order to confirm or not these preliminary results, we note that a potential source of systematic bias can be hidden in our estimator of the effective Seebeck coefficient. To obtain S_{eff}, both the temperature and the electrical potential have been averaged over cross sections of the geometry. Because of the random nature of the oxide inclusions, the isosurfaces of both temperature and electrical potential are not necessarily parallel to the cross sections. As a consequence, the averages may strongly depend on the location of the cross sections. This is in principle a statistical issue which can be fixed by devising a more robust averaging procedure. Research in this direction is ongoing.

REFERENCES

[1]   X. Liu *et al.*, "State of the art in composition, fabrication, characterization, and modeling methods of cement-based thermoelectric materials for low-temperature applications," *Renewable and Sustainable Energy Reviews,* vol. 137, p. 110361, 2021/03/01/ 2021, doi: https://doi.org/10.1016/j.rser.2020.110361.

[2]   X. Wang, S. Dong, A. Ashour, and B. Han, "Energy-harvesting concrete for smart and sustainable infrastructures," *Journal of Materials Science,* vol. 56, no. 29, pp. 16243-16277, 2021/10/01 2021, doi: 10.1007/s10853-021-06322-1.

[3]   S. Ding, S. Dong, A. Ashour, and B. Han, "Development of sensing concrete: Principles, properties and its applications," *Journal of Applied Physics,* vol. 126, no. 24, p. 241101, 2019, doi: 10.1063/1.5128242.

[4]   D. D. L. Chung, "Composites get smart," *Materials Today,* vol. 5, no. 1, pp. 30-35, 2002/01/01/ 2002, doi: https://doi.org/10.1016/S1369-7021(02)05140-4.

[5]   N. Cusack and P. Kendall, "The Absolute Scale of Thermoelectric Power at High Temperature," *Proceedings of the Physical Society,* vol. 72, no. 5, pp. 898-901, 1958/11/01 1958, doi: 10.1088/0370-1328/72/5/429.

[6]   R. Jani *et al.*, "Characterization and performance of cement-based thermoelectric materials," *Civil Engineering Research in Ireland (CERI) 2020,* 2020.

[7]   S. Wen and D. D. L. Chung, "Seebeck effect in carbon fiber-reinforced cement," *Cement and Concrete Research,* vol. 29, no. 12, pp. 1989-1993, 1999/12/01/ 1999, doi: https://doi.org/10.1016/S0008-8846(99)00185-4.

[8]   S. Wen and D. D. L. Chung, "Erratum to "Seebeck effect in carbon fiber reinforced cement"," *Cement and Concrete Research,* vol. 34, no. 12, pp. 2341-2342, 2004/12/01/ 2004, doi: https://doi.org/10.1016/j.cemconres.2004.01.010.

[9]   J. Wei, L. Zhao, Q. Zhang, Z. Nie, and L. Hao, "Enhanced thermoelectric properties of cement-based composites with expanded graphite for climate adaptation and large-scale energy harvesting," *Energy and Buildings,* vol. 159, pp. 66-74, 2018/01/15/ 2018, doi: https://doi.org/10.1016/j.enbuild.2017.10.032.

[10]   J. Wei, Z. Nie, G. He, L. Hao, L. Zhao, and Q. Zhang, "Energy harvesting from solar irradiation in cities using the thermoelectric behavior of carbon fiber reinforced cement composites," *RSC Advances,* 10.1039/C4RA07864K vol. 4, no. 89, pp. 48128-48134, 2014, doi: 10.1039/C4RA07864K.

[11]   J. Wei, Q. Zhang, L. Zhao, L. Hao, and Z. Nie, "Effect of moisture on the thermoelectric properties in expanded graphite/carbon fiber cement composites," *Ceramics International,* vol. 43, no. 14, pp. 10763-10769, 2017/10/01/ 2017, doi: https://doi.org/10.1016/j.ceramint.2017.05.088.

[12]   J. Wei, L. Hao, G. He, and C. Yang, "Enhanced thermoelectric effect of carbon fiber reinforced cement composites by metallic oxide/cement interface," *Ceramics International,* vol. 40, no. 6, pp. 8261-8263, 2014/07/01/ 2014, doi: https://doi.org/10.1016/j.ceramint.2014.01.024.

[13]   J. Wei, Q. Zhang, L. Zhao, L. Hao, and C. Yang, "Enhanced thermoelectric properties of carbon fiber reinforced cement composites," *Ceramics International,* vol. 42, no. 10, pp. 11568-11573, 2016/08/01/ 2016, doi: https://doi.org/10.1016/j.ceramint.2016.04.014.

[14]   T. Ji, X. Zhang, X. Zhang, Y. Zhang, and W. Li, "Effect of Manganese Dioxide Nanorods on the Thermoelectric Properties of Cement Composites," *Journal of Materials in Civil Engineering,* vol. 30, no. 9, p. 04018224, 2018, doi: doi:10.1061/(ASCE)MT.1943-5533.0002401.

[15] T. Ji, S. Zhang, Y. He, X. Zhang, X. Zhang, and W. Li, "Enhanced thermoelectric property of cement-based materials with the synthesized MnO2/carbon fiber composite," *Journal of Building Engineering,* vol. 43, p. 103190, 2021/11/01/ 2021, doi: https://doi.org/10.1016/j.jobe.2021.103190.

[16] I. Vareli *et al.*, "High-performance cement/SWCNT thermoelectric nanocomposites and a structural thermoelectric generator device towards large-scale thermal energy harvesting," *Journal of Materials Chemistry C,* 10.1039/D1TC03495B vol. 9, no. 40, pp. 14421-14438, 2021, doi: 10.1039/D1TC03495B.

[17] R. Landauer, "Electrical conductivity in inhomogeneous media," *AIP Conference Proceedings,* vol. 40, no. 1, pp. 2-45, 1978, doi: 10.1063/1.31150.

[18] D. S. McLachlan, M. Blaszkiewicz, and R. E. Newnham, "Electrical Resistivity of Composites," *Journal of the American Ceramic Society,* vol. 73, no. 8, pp. 2187-2203, 1990, doi: https://doi.org/10.1111/j.1151-2916.1990.tb07576.x.

[19] J. B. Vaney *et al.*, "Effective medium theory based modeling of the thermoelectric properties of composites: comparison between predictions and experiments in the glass–crystal composite system Si10As15Te75–Bi0.4Sb1.6Te3," *Journal of Materials Chemistry C,* 10.1039/C5TC02087E vol. 3, no. 42, pp. 11090-11098, 2015, doi: 10.1039/C5TC02087E.

[20] J. Sonntag, "Comment on "Effective medium theory based modeling of the thermoelectric properties of composites: comparison between predictions and experiments in the glass–crystal composite system Si10As15Te75–Bi0.4Sb1.6Te3" by J.-B. Vaney et al., J. Mater. Chem. C, 2015, 3, 11090," *Journal of Materials Chemistry C,* 10.1039/C6TC03140D vol. 4, no. 46, pp. 10973-10976, 2016, doi: 10.1039/C6TC03140D.

[21] J. Sonntag, B. Lenoir, and P. Ziolkowski, "Electronic Transport in Alloys with Phase Separation (Composites)," *Open Journal of Composite Materials,* 2019.

[22] X. Hu *et al.*, "Power generation from nanostructured PbTe-based thermoelectrics: comprehensive development from materials to modules," *Energy & Environmental Science,* 10.1039/C5EE02979A vol. 9, no. 2, pp. 517-529, 2016, doi: 10.1039/C5EE02979A.

[23] K. Huang and F. Edler, "Multiphysics Simulation of Seebeck Coefficient Measurement," *Journal of Electronic Materials,* vol. 51, no. 6, pp. 3276-3287, 2022/06/01 2022, doi: 10.1007/s11664-022-09577-9.

[24] G. Wu and X. Yu, "A holistic 3D finite element simulation model for thermoelectric power generator element," *Energy Conversion and Management,* vol. 86, pp. 99-110, 2014/10/01/ 2014, doi: https://doi.org/10.1016/j.enconman.2014.04.040.

[25] M. Jaegle, "Multiphysics simulation of thermoelectric systems-modeling of Peltier-cooling and thermoelectric generation," in *COMSOL Conference 2008 Hannover*, 2008, no. 6.

[26] E. E. Antonova and D. C. Looman, "Finite elements for thermoelectric device analysis in ANSYS," in *ICT 2005. 24th International Conference on Thermoelectrics, 2005.*, 19-23 June 2005 2005, pp. 215-218, doi: 10.1109/ICT.2005.1519922.

[27] G. Wu and X. Yu, "A Comprehensive 3D Finite Element Model of a Thermoelectric Module Used in a Power Generator: A Transient Performance Perspective," *Journal of Electronic Materials,* vol. 44, no. 6, pp. 2080-2088, 2015/06/01 2015, doi: 10.1007/s11664-015-3664-1.

[28] X. Hu, H. Takazawa, K. Nagase, M. Ohta, and A. Yamamoto, "Three-Dimensional Finite-Element Simulation for a Thermoelectric Generator Module," *Journal of Electronic Materials,* vol. 44, no. 10, pp. 3637-3645, 2015/10/01 2015, doi: 10.1007/s11664-015-3898-y.

[29] D. Ebling, M. Jaegle, M. Bartel, A. Jacquot, and H. Böttner, "Multiphysics Simulation of Thermoelectric Systems for Comparison with Experimental Device Performance," *Journal of Electronic Materials,* vol. 38, no. 7, pp. 1456-1461, 2009/07/01 2009, doi: 10.1007/s11664-009-0825-0.

[30] B. M. Warnes, F. F. Aplan, and G. Simkovich, "Electrical conductivity and seebeck voltage of Fe2O3, pure and doped, as a function of temperature and oxygen pressure," *Solid State Ionics,* vol. 12, pp. 271-276, 1984/03/01/ 1984, doi: https://doi.org/10.1016/0167-2738(84)90156-5.

[31] A. I. Ansel'm, *Introduction to semiconductor theory*. Mir Publishers, 1981.

[32] *COMSOL Multiphysics® v. 6.0*. COMSOL AB, Stockholm, Sweden. [Online]. Available: www.comsol.com

[33] S. Angst and D. E. Wolf, "Network theory for inhomogeneous thermoelectrics," *New Journal of Physics,* vol. 18, no. 4, p. 043004, 2016/04/04 2016, doi: 10.1088/1367-2630/18/4/043004.

[34] A. G. Rösch *et al.*, "Improved Electrical, Thermal, and Thermoelectric Properties Through Sample-to-Sample Fluctuations in Near-Percolation Threshold Composite Materials," *Advanced Theory and Simulations,* vol. 4, no. 6, p. 2000284, 2021, doi: https://doi.org/10.1002/adts.202000284.